Title

Individual connectomes are unique and stable in the developing brain from adolescence to young adulthood.

Corey Horien[a], Xilin Shen[b], Dustin Scheinost[b,c], R. Todd Constable[a,b,d]

[a]Interdepartmental Neuroscience Program, Yale University School of Medicine, New Haven, CT

[b]Department of Radiology and Biomedical Imaging, Yale University School of Medicine, New Haven, CT

[c]The Child Study Center, Yale University School of Medicine, New Haven, CT

[d]Department of Neurosurgery, Yale University School of Medicine, New Haven, CT

*Corresponding author:

Corey Horien

Magnetic Resonance Research Center

300 Cedar St

PO Box 208043

New Haven, CT 06520-8043

Tel: (203) 785-6148

corey.horien@yale.edu

Abstract

Using fMRI and functional connectivity analyses, it is possible to establish a functional connectome for an individual. The extent to which functional connectomes from adolescents and young adults remain identifiable across many years has not been investigated. Here we show in three publically available longitudinal resting-state fMRI datasets that connectome-based identification of adolescents and young adults scanned 1-3 years apart is possible at levels well above chance using whole-brain functional connectivity data. When we restrict the identification process to specific edges, we find that edges in the frontal, parietal, and temporal cortices tend to lead to the highest identification rates. We also demonstrate that highly unique edges contributing the most to a successful ID tend to connect nodes in these same cortical regions, while edges contributing the least tend to connect cross-hemispheric homologs. These results suggest that despite developmental changes, adolescent and young adult subjects have unique and stable functional connectomes and that the frontal, parietal, and temporal cortices are important in defining individual uniqueness in younger subjects.

Introduction

Using fMRI and functional connectivity (FC) analyses, it is possible to establish a functional connectome for an individual. It has previously been shown that young adults' functional connectomes are unique and stable across multiple days (Finn et al., 2015). This uniqueness and stability allows for the identification of an individual from a pool of other individuals. The ability to identify individuals via their functional connectome after multiple days has been replicated many times in adult subjects (Biazoli et al., 2017; Finn et al., 2017; Horien et al., 2017; Noble et al., 2017; Vanderwal et al., 2017; Waller et al., 2017). In addition, it

has also been demonstrated that children and young adults have a unique functional connectome that allows identification even across different task conditions (Kaufmann et al., 2017).

However, questions remain as to the stability of the functional connectome over longer periods of time and also as to when in the developmental trajectory the connectome becomes unique. To date all identification studies have used data in which subjects were scanned only days apart - or in some cases, on the same day. Hence, the extent to which the individual functional connectome remains unique across longer time intervals, such as years, and in periods of large brain changes, such as adolescence, is still unclear.

Using three publically available resting-state fMRI (rs-fMRI) datasets in which subjects were scanned years apart, we investigated if the individual connectome of an adolescent or young adult (age range: 10-23) is unique and retains its uniqueness across longer time frames (1-3 years). We also investigated the relative stability of an individual's functional connectivity patterns over time and identified the portions of the brain that are important for individual uniqueness. We hypothesized that individual connectomes will be unique across development over several years, despite substantial changes in development and the associated changes in connectivity.

Methods

Description of datasets

We utilized three longitudinal rs-fMRI datasets of neurotypical subjects. The University of Pittsburgh School of Medicine dataset and the University of Utah dataset (hereafter referred to as Pitt and Utah, respectively) were downloaded from the Consortium for Reliability and Reproducibility (CoRR; http://fcon_1000.projects.nitrc.org/indi/CoRR/html/samples.html; Zuo et al., 2014); the Southwest University Longitudinal Imaging Multimodal dataset (hereafter

referred to as SLIM; Liu et al., 2017) was downloaded through the International Data-sharing Initiative (INDI; http://fcon_1000.projects.nitrc.org/). Subjects were excluded from the SLIM and Pitt datasets due to incomplete brain coverage in the functional scan (mostly in the cerebellum), and in the case of the SLIM data subjects had to have data from all three scans. All datasets were collected in accordance with the institutional review board or research ethics committee at each site. All resting-state scans were acquired on Siemens 3-T Trio scanners. Relevant demographic characteristics and imaging parameters are described in Table 1; full details of the Pitt and SLIM datasets can be found elsewhere (Hwang, Hallquist, & Luna, 2013; Liu et al., 2017). Note that because of numerous differences between the datasets (eyes open/closed during rest, resting-state scan collected after other functional runs, number of years between scans, etc.) we are not interested in comparing ID rates between datasets; rather, we are interested in defining the upper bounds of identifiability in each dataset.

Preprocessing

The preprocessing strategy used has been described in detail elsewhere (Noble et al., 2017). All analyses were performed using BioImage Suite (Joshi et al., 2011) unless otherwise indicated. We note that we only preprocessed the Pitt and Utah subjects, as the SLIM data was preprocessed beforehand; for SLIM, we downloaded (http://fcon_1000.projects.nitrc.org/indi/retro/southwestuni_qiu_index.html) pre-calculated connectivity matrices that were generated using an approach similar to what we detail below. For preprocessing, briefly, we skull-stripped the magnetization prepared rapid gradient echo (MPRAGE) images using optiBET (Lutkenhoff et al., 2014) and performed linear and non-linear transformations to warp a 268 node functional atlas from MNI space to single subject space using BioImage Suite as in Noble et al. (2017). Functional images were slice-time and motion

corrected using SPM5 (http://www.fil.ion.ucl.ac.uk/spm/software/spm5/). Covariates of no interest were regressed from the data, including linear, quadratic, and cubic drift, 24 motion parameters, mean cerebral-spinal fluid (CSF) signal, mean white matter signal, and the overall global signal. Data were temporally smoothed with a zero-mean unit-variance Gaussian filter (approximate cutoff frequency of 0.12 Hz).

Node and network definition

We used a 268 node functional atlas described previously (Finn et al., 2015). For each subject the average timecourse of each region of interest (node in graph theoretic terminology) was calculated, and the Pearson correlation coefficient was calculated between every other node to achieve a symmetric 268 x 268 matrix of correlation values representing edges (connections between nodes) in graph theoretic terminology. We subsequently normalized the matrix to z-scores via a Fisher transformation and only considered the upper triangle of the matrix, giving 35,778 unique edges for whole-brain analyses. These nodes were then grouped into 10 functional networks as in Finn et al. (2015). Network names are listed in Figure 2a.

We note that in the SLIM and Pitt datasets, even after excluding subjects missing significant amounts of data in the functional scan, many subjects were still missing edges in the whole-brain connectivity matrix due to incomplete coverage. To ensure standardization within a dataset, if a remaining subject was missing an edge, we removed that edge from all subjects. Of the 35,778 edges in the whole-brain functional connectome, 31,626 edges/subject remained in the SLIM dataset; 29,646 edges/subject remained in the Pitt dataset. All 35,778 edges were covered for all subjects in the Utah dataset. See Supplemental Figure 1 for the proportion of edges remaining in network pairs for SLIM and Pitt.

Identification procedure

The identification procedure has been described in detail previously (Finn et al., 2015). Briefly, a database is first created consisting of all the subjects' connectivity matrices from a particular session for a specific dataset (for example, session 2 Pitt). In an iterative process, a connectivity matrix from a particular subject is then selected from a different session and denoted as the target (for example, subject 1 in session 1 Pitt). Pearson correlation coefficients are then calculated between the target connectivity matrix and all the matrices (across all subjects) in the database from session 2. If the highest Pearson correlation coefficient is between subject 1 in one session and subject 1 in the second session, this would be recorded as a correct identification. Subject 2 from session 1 would then be denoted as the target, and the algorithm would continue with the same database of subjects. This continues until identifications have been performed for all subjects, sessions, and database-target combinations. Statistical significance was assessed via permutation testing, in which a null distribution is generated by randomly shuffling subject identities and performing the identification procedure with the incorrect labels. We obtained whole-brain based identification results for all subjects with no motion exclusion criteria; we also performed identification with subjects grouped according to gender and motion (a mean frame-frame displacement (FFD) threshold of 0.1 mm; if either scan session had a value above 0.1 mm, this subject was denoted as a high motion subject). We also investigated how specific within- and between-network edges, as well as a combination of networks, affected the identification analyses. In this approach, only the edges comprising the network(s) of interest were used for identification. To compare ID rates between networks in a dataset we performed 1000 bootstraps with ~80% of the subjects to generate 95% confidence intervals and determine significance.

To ensure that identification was not due to idiosyncratic head movements specific to an individual across sessions, we conducted identification analyses using estimates of head movement parameters which has been described in detail elsewhere (Finn et al., 2015). Briefly, we calculated discrete motion distribution vectors for each subject based on FFD over an entire scan. We then computed the mean and standard deviations of the FFD across all subjects for each dataset. We then specified 15 bins for the Utah and SLIM subjects and 10 bins for the Pitt subjects to span the grand mean +/- 3 standard deviations, and motion distribution vectors were subsequently calculated. These vectors were then submitted to the identification procedure.

Edge-based and linear regression analyses

To determine the role of specific edges in the identification process, we performed calculations to quantify highly unique and highly consistent edges via the differential power (DP) measure and the group consistency measure described in detail elsewhere (Finn et al., 2015); we provide a brief overview here. DP estimates for each given edge the likelihood that within subject similarity is higher than similarity measured across different subjects. The product of edge values from time 1 and time 2 from the same subject is compared to product of time 1 and time 2 from unmatched subjects. Edges with high DP values are considered helpful in identification. To calculate the group consistency measure, we multiply an edge value from time 1 and time 2 across all edges for all subjects and calculate the mean for each edge. Edges with high values in this measure are therefore high across all individuals in the group and are not helpful in identification. In the course of these analyses, we also determined the network pair the edges belong to (within- and between-networks); to account for differences in network sizes in both of these analyses, we divided the number of significant edges in a network pair by the number of total edges in the network.

To investigate the relationship between within-subject correlation scores (self-correlation), age, and time between scans, we performed linear regression analyses between self-correlation and the number of days between scans; we also correlated self-correlation scores with age. We further performed partial correlation analyses in which we assessed the relationship between self-correlation scores and age while controlling for time between scans and vice-versa.

Results

Whole-brain identification results

Using the whole-brain connectivity matrix, we were able to identify subjects at rates highly above chance in all three datasets (Figure 1a). For example, the lowest identification rate we achieved was 43.3 percent, which is still well above chance ($P < 0.0001$). Success rates ranged from 43.3%, in the Pitt session 1-session 3 identification, to 84.6%, in the Utah session 1-session 2B identification. The high accuracy rates do not appear to be driven by subject-specific in-scanner motion, as the highest ID rates we obtained based on each subject's motion distribution vector were 1.92%, 2.9%, and 4.3% for Utah, SLIM, and Pitt, respectively.

Identification was also performed after grouping subjects according to gender and a 0.1 mm mean frame-frame displacement (FFD) threshold used to split subjects into high and low motion groups. We observed no sex effect in identification rates among males versus females, though we noted consistently higher rates among the low motion group compared to the high motion group (Supplemental Figure 2). Of note, all the rates we obtained from all whole-brain based analyses were highly above chance ($P < 0.0001$).

Within-subject correlation scores, age, and time between scan results

We next investigated the relationship between self-correlation scores (the correlation of a subject from time 1 to time 2), age, and years in between scans by performing linear regression

analyses. In general, when all subjects were included in the analysis (i.e. when we do not apply the motion threshold used above) there appears to be a negative correlation between self-correlation and years between scans, though none of these results were statistically significant (all $P > 0.05$; Figure 1b). Similarly, investigating self-correlation versus age (Figure 1c) again indicated no clear relationship, with the only significant result coming from Pitt session1-session2 subjects ($r = 0.2323$, $P = 0.025$).

To investigate if there were systematic differences in self-correlation between subjects due to motion or gender that might go undetected in the identification algorithm, we performed the same linear regression analyses as above except grouped subjects either by sex or the 0.1 mm mean FFD threshold. No obvious differences due to either emerged (Supplemental Figures 3 and 4). In addition, we performed partial correlation analyses to explore the relationship between self-correlation and years between scans while controlling for age (and vice-versa). With the exception of Pitt session 1-session 2 (self-correlation versus age while controlling for years between scans; *rho* = 0.2298; $P = 0.0276$), all analyses yielded non-significant results (Supplemental Table 1), As a final check, we also correlated subject age with time between scans. We did find significant negative correlations in time between scans and age in SLIM session 1-session 2 and session 1-session 3 ($r = -0.3424$, $P = 3.503e-04$; $r = -0.3921$, $P = 3.5159e-05$); all other correlations were not significant. Taken together, the results of these analyses reinforce that self-correlation scores we analyzed here tend to be stable between scans, there is no clear relationship between self-correlation and age, and our results do not seem to be driven by factors like gender, motion, or other confounding variables. Therefore, to increase the difficulty of the identification process, we performed the remainder of the analyses on all subjects in a given dataset (i.e. we did not group subjects by gender or motion). We also restrict

our analyses to session 1 – session 2, given that these session pairs had the largest sample sizes (note we used Utah 2A as the second session in this dataset).

Network-based identification results

Having determined whole-brain connectivity data is stable across years, we next tested the contributions to this stability of specific within- and between-network pairs. We grouped the connectivity data for each subject into 10 functional networks (Figure 2a), and subsequently performed identification analyses using only the edges from a given network pair. In general, we observed edges within or between the medial frontal and frontoparietal networks (networks 1 and 2, respectively), tended to lead to the highest identification rates for all three datasets, with network 3 (default mode network) edges also leading to high ID rates (Figure 2b) consistent with the original fingerprinting work of Finn et al. (2015). In addition, when we only considered the within-network edges and combined networks 1 and 2, we tended to achieve even higher ID rates than when using only the network pairs in isolation. For example, considering the 45 between-network and 10 within-network identifications for each dataset, the combined network 1 and 2 ID rate was higher than 51/55 network pairs for Utah ($P < 0.05$); for 52/55 network pairs for Pitt ($P < 0.05$); and for 53/55 network pairs for SLIM ($P < 0.05$), again echoing the results of Finn et al. (2015) and emphasizing the importance of medial frontal and frontoparietal networks (see Supplemental Table 2 for actual rates obtained and non-significant network pairs). Despite the different ID rates achieved, however, we note that identification was still highly significant across all network pairs (i.e. ID rates were well above chance even for the worst performing networks): of the 165 network-based identifications we performed for session 1-session 2 (45 between-network and 10 within-network identifications for each dataset; 55 x 3 datasets = 165 identifications), 162 had $P <0.001$, 2 had $P = 0.006$, and 1 had $P = 0.002$.

Edge-based analyses results

Lastly, we assessed the importance of specific edges to subject uniqueness. Using the DP measure, which calculates how characteristic an edge tends to be, we were able to determine which edges were important in the identification process. A representative example from SLIM showing the anatomic location of the edges from this analysis is provided (Figure 3a). The results were consistent across all three datasets and a range of thresholds (data not shown). In general, highly discriminative edges tend to cluster in the prefrontal, parietal, and temporal cortices. To determine relative network representation, we calculated the number of significant edges present in a network pair. DP edges tended to be located within or between networks 1 and 2 and to a lesser extent network 3; representation was also found in other regions, though at somewhat lower levels (Figure 3b). As an example of the relative over-representation of significant edges in the medial frontal and frontoparietal regions, after averaging the three matrices calculated from session 1-session 2 (shown as the average matrix in Figure 3b), we found approximately 60% of the edges were located within networks 1 and 2 or connecting these networks to other regions.

To quantify the extent to which individual edges do not contribute to subject uniqueness, we calculated the group consistency measure, which quantifies edges that are highly consistent within a single subject and across all subjects in a dataset. Because they are highly consistent for all subjects in a dataset, they do not discriminate between individuals. A representative example showing the anatomic location of the edges from this analysis is shown (Figure 3c). Results, consistent across all three datasets and a range of thresholds (data not shown), revealed that edges contributing the least to identification tended to link cross-hemispheric homologs (Figure 3d). By averaging the matrices from session 1-session 2 for all datasets (shown in Figure 3d), we

found approximately 67% of the edges were within visual 1 and visual 2 networks (networks 5 and 6, respectively).

Discussion

An unexpected finding from the HCP project was that the functional connectome is unique for each individual, and it has been an open question as to what extent the connectome remains identifiable over weeks, months or years, including through periods of significant brain development (Finn et al., 2015; Finn & Constable, 2016). Here we demonstrate in adolescents and young adults that an individual's functional connectome remains unique and relatively stable for at least three years. To the best of our knowledge, this is the first time successful connectome-based identification has been demonstrated in datasets in which participants were scanned years apart. While the high identifiability we achieved is consistent with earlier studies performed in adult subjects (although age ranges vary for these studies, most participants tend to be in the 20–35 year old range; (Finn et al., 2017; Finn et al., 2015; Horien et al., 2017 Noble et al., 2017; Vanderwal et al., 2017; Waller et al., 2017), and also in line with the observations of Kauffman et al. (2017) in younger subjects (8–22 year olds), all of these studies have been cross-sectional in nature. Because of the longitudinal aspect of the datasets analyzed here, we extend the earlier observations by showing that unique FC patterns are stable at longer time scales.

By performing our analyses in adolescents and young adults who are experiencing both structural and functional changes in brain development (Brenhouse & Andersen, 2011; Burnett, Sebastian, Cohen Kadosh, & Blakemore, 2011; Casey, Giedd, & Thomas, 2000; Casey & Jones, 2010; Casey, Jones, & Hare, 2008; Casey et al., 2010; Giedd et al., 2009; Giedd & Rapoport, 2010; Gogtay et al., 2004; Johnson, Blum, & Giedd, 2009; Tamnes et al., 2013; Tau & Peterson, 2010), in principle a successful identification should be more difficult. Nevertheless, we were

still able to successfully predict the identities of individuals at levels highly above chance using the functional connectome. Our results suggest that there is an inherent stability in the connectome and that unique patterns of FC endure even during adolescent development. While the idea of stability in the developing brain might seem counterintuitive, the multivariate nature of the identification procedure helps explain our results. For example, it has been reported that univariate measures of FC (i.e. individual edges) change in strength across longitudinal scans (Noble et al., 2017; Pannunzi et al., 2017) and are expected to change across development, but these changes are evidently not enough to overcome the large-scale, subject-specific patterns in FC that allow high within-subject correlations and a successful identification. Our results are thus consistent with the presence of an FC organizational structure that is stable through development, an idea that has been suggested based on the similarity of neonatal connectomes to mature adult connectomes (van den Heuvel et al., 2015).

We also demonstrate through network-based identification and edge-based analyses that the medial frontal, frontoparietal, and default mode networks were most discriminative of adolescent and young adult subjects across longer time scales. Given that these networks undergo developmental changes (de Bie et al., 2012; Fair et al., 2008; Gu et al., 2015; Sato et al., 2014; Sherman et al., 2014; Supekar et al., 2010), our results again might seem counterintuitive. However, recent studies have shown that connectomes from children are generally similar to adults in terms of overall network structure (Fair et al., 2012; Marek, Hwang, Foran, Hallquist, & Luna, 2015; Power, Barnes, Snyder, Schlaggar, & Petersen, 2012), providing evidence that despite changes in FC, large-scale patterns in brain networks are still similar across development. Together with the high identifiability we observed, this suggests that subject-specific patterns in these highly distinctive networks are present even in younger individuals.

Our results are also consistent with a number of factors emerging as important in the connectome-based identification and reliability literature. We obtained consistently higher ID rates when restricting analyses to only low-motion subjects. While the inherent decrease in sample size when using a within-dataset motion-threshold makes direct comparison of ID rates difficult (i.e. samples in this study were essentially cut in half when we used a motion cutoff), the effect of motion on ID rates we observed is consistent with other work (Horien et al., 2017). Further, the importance of scan time on within-subject reliability scores (like connectivity-based identification) is increasingly being recognized (Airan et al., 2016; Birn et al., 2013; Finn et al., 2017; Finn et al., 2015; Laumann et al., 2015; Mueller et al., 2015; Noble et al., 2017; Shah, Cramer, Ferguson, Birn, & Anderson, 2016), and we observed that the Pitt dataset, with only 5 minutes of data per subject, tended to have lower rates of identification relative to the other datasets (8 minutes of data each). Numerous differences among the datasets (i.e. differences in developmental stage of subjects, number of years between scans, eyes open versus closed during rest, etc.) could also explain these findings, however, so further work is needed.

A number of other questions remain open for study. The youngest subjects we studied were approximately 10 years old. Establishing when an individual's unique functional connectome profile emerges should be examined, as well as when connectome uniqueness breaks down. Studies in adults have shown identification rates are highest when subjects are completing a task in the scanner (possibly by increasing subject-specific signal-to-noise and augmenting unique patterns of FC; Finn et al., 2017; Vanderwal et al., 2017), so identifiability should be investigated when younger subjects are completing task-based scans to see if a similar pattern holds. Since reliability of functional neuroimaging data is a topic of increasing interest, the extent to which other measures of reliability map onto the developing brain should be

examined. Finally, future work should determine if the stability of fMRI connectivity data allows predictions to be made regarding behavior at longer time frames, similar to how previous investigators have used FC measures to predict a behavioral or psychiatric score in cross-sectional studies (Drysdale et al., 2017; Finn et al., 2015; Hearne, Mattingley, & Cocchi, 2016; Kaufmann et al., 2017; Rosenberg et al., 2016; Shen et al., 2017).

In sum, we have shown adolescent and young adult subjects have unique and stable functional connectomes and that the frontal, parietal, and temporal cortices are important in defining individual uniqueness in younger subjects. Leveraging the stability of FC data in younger subjects to generate meaningful models related to behavior and cognition remains an important next step of study.

Acknowledgements

This work was supported by a Medical Scientist Training Program training grant (NIH/NIGMS T32GM007205; C.H.)

References

Airan, R. D., Vogelstein, J. T., Pillai, J. J., Caffo, B., Pekar, J. J., & Sair, H. I. (2016). Factors affecting characterization and localization of interindividual differences in functional connectivity using MRI. *Hum Brain Mapp, 37*(5), 1986-1997.

Biazoli, C. E., Jr., Salum, G. A., Pan, P. M., Zugman, A., Amaro, E., Jr., Rohde, L. A., et al. (2017). Commentary: Functional connectome fingerprint: identifying individuals using patterns of brain connectivity. *Front Hum Neurosci, 11*, 47.

Birn, R. M., Molloy, E. K., Patriat, R., Parker, T., Meier, T. B., Kirk, G. R., et al. (2013). The effect of scan length on the reliability of resting-state fMRI connectivity estimates. *Neuroimage, 83*, 550-558.

Brenhouse, H. C., & Andersen, S. L. (2011). Developmental trajectories during adolescence in males and females: a cross-species understanding of underlying brain changes. *Neurosci Biobehav Rev, 35*(8), 1687-1703.

Burnett, S., Sebastian, C., Cohen Kadosh, K., & Blakemore, S. J. (2011). The social brain in adolescence: evidence from functional magnetic resonance imaging and behavioural studies. *Neurosci Biobehav Rev, 35*(8), 1654-1664.

Casey, B. J., Giedd, J. N., & Thomas, K. M. (2000). Structural and functional brain development and its relation to cognitive development. *Biol Psychol, 54*(1-3), 241-257.

Casey, B. J., & Jones, R. M. (2010). Neurobiology of the adolescent brain and behavior: implications for substance use disorders. *J Am Acad Child Adolesc Psychiatry, 49*(12), 1189-1201; quiz 1285.

Casey, B. J., Jones, R. M., & Hare, T. A. (2008). The adolescent brain. *Ann N Y Acad Sci, 1124*, 111-126.

Casey, B. J., Jones, R. M., Levita, L., Libby, V., Pattwell, S. S., Ruberry, E. J., et al. (2010). The storm and stress of adolescence: insights from human imaging and mouse genetics. *Dev Psychobiol, 52*(3), 225-235.

de Bie, H. M., Boersma, M., Adriaanse, S., Veltman, D. J., Wink, A. M., Roosendaal, S. D., et al. (2012). Resting-state networks in awake five- to eight-year old children. *Hum Brain Mapp, 33*(5), 1189-1201.

Drysdale, A. T., Grosenick, L., Downar, J., Dunlop, K., Mansouri, F., Meng, Y., et al. (2017). Resting-state connectivity biomarkers define neurophysiological subtypes of depression. *Nat Med, 23*(1), 28-38.

Fair, D. A., Cohen, A. L., Dosenbach, N. U., Church, J. A., Miezin, F. M., Barch, D. M., et al. (2008). The maturing architecture of the brain's default network. *Proc Natl Acad Sci U S A, 105*(10), 4028-4032.

Fair, D. A., Nigg, J. T., Iyer, S., Bathula, D., Mills, K. L., Dosenbach, N. U., et al. (2012). Distinct neural signatures detected for ADHD subtypes after controlling for micro-movements in resting-state functional connectivity MRI data. *Front Syst Neurosci, 6*, 80.

Finn, E. S., Scheinost, D., Finn, D. M., Shen, X., Papademetris, X., & Constable, R. T. (2017). Can brain state be manipulated to emphasize individual differences in functional connectivity? *Neuroimage*.

Finn, E. S., Shen, X., Scheinost, D., Rosenberg, M. D., Huang, J., Chun, M. M., et al. (2015). Functional connectome fingerprinting: identifying individuals using patterns of brain connectivity. *Nat Neurosci, 18*(11), 1664-1671.

Finn, E. S., & Todd Constable, R. (2016). Individual variation in functional brain connectivity: implications for personalized approaches to psychiatric disease. *Dialogues Clin Neurosci, 18*(3), 277-287.

Giedd, J. N., Lalonde, F. M., Celano, M. J., White, S. L., Wallace, G. L., Lee, N. R., et al. (2009). Anatomical brain magnetic resonance imaging of typically developing children and adolescents. *J Am Acad Child Adolesc Psychiatry, 48*(5), 465-470.

Giedd, J. N., & Rapoport, J. L. (2010). Structural MRI of pediatric brain development: what have we learned and where are we going? *Neuron, 67*(5), 728-734.

Gogtay, N., Giedd, J. N., Lusk, L., Hayashi, K. M., Greenstein, D., Vaituzis, A. C., et al. (2004). Dynamic mapping of human cortical development during childhood through early adulthood. *Proc Natl Acad Sci U S A, 101*(21), 8174-8179.

Gu, S., Satterthwaite, T. D., Medaglia, J. D., Yang, M., Gur, R. E., Gur, R. C., et al. (2015). Emergence of system roles in normative neurodevelopment. *Proc Natl Acad Sci U S A, 112*(44), 13681-13686.

Hearne, L. J., Mattingley, J. B., & Cocchi, L. (2016). Functional brain networks related to individual differences in human intelligence at rest. *Sci Rep, 6*, 32328.

Horien, C., Noble, S., Finn, E. S., Shen, X., Scheinost, D., & Constable, R. T. (2017). Considering factors affecting the connectome-based identification process: Comment on Waller et al. *Neuroimage*.

Hwang, K., Hallquist, M. N., & Luna, B. (2013). The development of hub architecture in the human functional brain network. *Cereb Cortex, 23*(10), 2380-2393.

Johnson, S. B., Blum, R. W., & Giedd, J. N. (2009). Adolescent maturity and the brain: the promise and pitfalls of neuroscience research in adolescent health policy. *J Adolesc Health, 45*(3), 216-221.

Joshi, A., Scheinost, D., Okuda, H., Belhachemi, D., Murphy, I., Staib, L. H., et al. (2011). Unified framework for development, deployment and robust testing of neuroimaging algorithms. *Neuroinformatics, 9*(1), 69-84.

Kaufmann, T., Alnaes, D., Doan, N. T., Brandt, C. L., Andreassen, O. A., & Westlye, L. T. (2017). Delayed stabilization and individualization in connectome development are related to psychiatric disorders. *Nat Neurosci, 20*(4), 513-515.

Laumann, T. O., Gordon, E. M., Adeyemo, B., Snyder, A. Z., Joo, S. J., Chen, M. Y., et al. (2015). Functional System and Areal Organization of a Highly Sampled Individual Human Brain. *Neuron, 87*(3), 657-670.

Liu, W., Wei, D., Chen, Q., Yang, W., Meng, J., Wu, G., et al. (2017). Longitudinal test-retest neuroimaging data from healthy young adults in southwest China. *Sci Data, 4*, 170017.

Lutkenhoff, E. S., Rosenberg, M., Chiang, J., Zhang, K., Pickard, J. D., Owen, A. M., et al. (2014). Optimized brain extraction for pathological brains (optiBET). *PLoS One, 9*(12), e115551.

Marek, S., Hwang, K., Foran, W., Hallquist, M. N., & Luna, B. (2015). The Contribution of Network Organization and Integration to the Development of Cognitive Control. *PLoS Biol, 13*(12), e1002328.

Mueller, S., Wang, D., Fox, M. D., Pan, R., Lu, J., Li, K., et al. (2015). Reliability correction for functional connectivity: Theory and implementation. *Hum Brain Mapp, 36*(11), 4664-4680.

Noble, S., Spann, M. N., Tokoglu, F., Shen, X., Constable, R. T., & Scheinost, D. (2017). Influences on the Test-Retest Reliability of Functional Connectivity MRI and its Relationship with Behavioral Utility. *Cereb Cortex*, 1-15.

Pannunzi, M., Hindriks, R., Bettinardi, R. G., Wenger, E., Lisofsky, N., Martensson, J., et al. (2017). Resting-state fMRI correlations: From link-wise unreliability to whole brain stability. *Neuroimage, 157*, 250-262.

Power, J. D., Barnes, K. A., Snyder, A. Z., Schlaggar, B. L., & Petersen, S. E. (2012). Spurious but systematic correlations in functional connectivity MRI networks arise from subject motion. *Neuroimage, 59*(3), 2142-2154.

Rosenberg, M. D., Finn, E. S., Scheinost, D., Papademetris, X., Shen, X., Constable, R. T., et al. (2016). A neuromarker of sustained attention from whole-brain functional connectivity. *Nat Neurosci, 19*(1), 165-171.

Sato, J. R., Salum, G. A., Gadelha, A., Picon, F. A., Pan, P. M., Vieira, G., et al. (2014). Age effects on the default mode and control networks in typically developing children. *J Psychiatr Res, 58*, 89-95.

Shah, L. M., Cramer, J. A., Ferguson, M. A., Birn, R. M., & Anderson, J. S. (2016). Reliability and reproducibility of individual differences in functional connectivity acquired during task and resting-state. *Brain Behav, 6*(5), e00456.

Shen, X., Finn, E. S., Scheinost, D., Rosenberg, M. D., Chun, M. M., Papademetris, X., et al. (2017). Using connectome-based predictive modeling to predict individual behavior from brain connectivity. *Nat Protoc, 12*(3), 506-518.

Sherman, L. E., Rudie, J. D., Pfeifer, J. H., Masten, C. L., McNealy, K., & Dapretto, M. (2014). Development of the default mode and central executive networks across early adolescence: a longitudinal study. *Dev Cogn Neurosci, 10*, 148-159.

Supekar, K., Uddin, L. Q., Prater, K., Amin, H., Greicius, M. D., & Menon, V. (2010). Development of functional and structural connectivity within the default mode network in young children. *Neuroimage, 52*(1), 290-301.

Tamnes, C. K., Walhovd, K. B., Dale, A. M., Ostby, Y., Grydeland, H., Richardson, G., et al. (2013). Brain development and aging: overlapping and unique patterns of change. *Neuroimage, 68*, 63-74.

Tau, G. Z., & Peterson, B. S. (2010). Normal development of brain circuits. *Neuropsychopharmacology, 35*(1), 147-168.

van den Heuvel, M. P., Kersbergen, K. J., de Reus, M. A., Keunen, K., Kahn, R. S., Groenendaal, F., et al. (2015). The Neonatal Connectome During Preterm Brain Development. *Cereb Cortex, 25*(9), 3000-3013.

Vanderwal, T., Eilbott, J., Finn, E. S., Craddock, R. C., Turnbull, A., & Castellanos, F. X. (2017). Individual differences in functional connectivity during naturalistic viewing conditions. *Neuroimage, 157*, 521-530.

Waller, L., Walter, H., Kruschwitz, J. D., Reuter, L., Muller, S., Erk, S., et al. (2017). Evaluating the replicability, specificity, and generalizability of connectome fingerprints. *Neuroimage, 158*, 371-377.

Zuo, X. N., Anderson, J. S., Bellec, P., Birn, R. M., Biswal, B. B., Blautzik, J., et al. (2014). An open science resource for establishing reliability and reproducibility in functional connectomics. *Sci Data, 1*, 140049.

Figure legends:

Figure 1. Connectome-based identification. Panel A: Results using whole brain data. Each dataset is indicated below the graph, along with the sessions that were involved in identification. Black shading indicates the early session served as the database session while the later session served as the target; gray shading indicates the later session served as the database with the early session serving as the target. “Average” refers to the average of all three datasets for each respective session identification pair. Panels B and C: Plotting self-correlation against years in between scans and age at scan time 1. Each dataset is indicated by the appropriate color and symbol. Results of linear regression analyses are shown on the appropriate graph.

Figure 2. Network-based identification. Panel A: Node and network labels. We utilized a 268-node functional atlas. Nodes were further grouped into the 10 functional networks indicated here.

Network names are to the left; anatomic locations are shown on the brains to the right. Panel B: We performed identification using only within- or between-network edges for session 1 and session 2 for all three datasets; shown are the average results for each database and target pair (i.e. a single element in the matrix represents the average identification rate of using session 1 as a database and session 2 as a target and vice-versa). "Average" above the right-most matrix refers to the average identification rate of all three datasets for session 1 and session 2 shown here. Note that because there were two scans in Utah session 2, we used session 2A in this analysis.

Figure 3. Results of edge-based analyses. Panel A: Anatomic location of highly unique (DP) edges from SLIM session 1-session 2. The edges shown here were in the top 99.9 percentile of highly unique edges. In the left two images of the brain, the red lines indicate edges connecting the red spheres, representing nodes. Nodes are sized according to degree, the number of edges connected to that node. On the right, the same nodes and edges are visualized on a circle plot, in which nodes are grouped according to anatomic location. The top of the circle represents anterior; the bottom, posterior. The left half of the circle plot corresponds to the left hemisphere of the brain. Panel B: Network representation of highly unique edges. Shown here are the data from the top 99.9 percentile of unique edges from session 1-session 2, as well as the average of all three datasets for session 1-session 2 shown here. Hotter colors indicate more edges are in the network pair. Note for both (B) and (D), the Utah session 2A scan was used. Panel C: Anatomic location of highly consistent (group consistency) edges from SLIM session 1-session 2. The edges shown here were in the top 99.9 percentile of highly consistent edges. Edges and nodes are represented as in (A). Panel D: Network representation of highly consistent edges. Shown here are the data from the top 99.9 percentile of highly consistent edges from session 1-session 2, as well as the average of all three datasets for session 1-session 2 shown here. The color scheme is as in (B). Note in (B) and (D) the scales of the color bars are not necessarily the same.

Table 1 legend: Demographic and imaging characteristics of datasets used in this study.

a. The subjects in Utah session 2 contain two runs, hereafter referred to as 2A and 2B.
b. Scan session 2 and 3 occurred on the same day in one female subject in this session; we removed it when conducting analyses that required us to incorporate the number of days between scans 2 and 3.
c. All datasets provided age in years at scan session 1. For SLIM and Utah, the ages were reported as integers in years only, while the time between scan sessions was reported in days. To standardize the reporting of age among all three datasets, we only report age at session 1 here.

Supplemental Figure 1. The number of edges remaining in network pairs in the SLIM and Pitt datasets. Each element in the matrix represents the number of edges remaining in that network pair divided by the number of edges present in the original network pair (i.e. if none are missing). All edges were present in Utah subjects.

Supplemental Figure 2. Identification results using whole brain data, grouping subjects according to gender or a 0.1 mm mean frame-frame displacement motion threshold. Shown here is the average identification for a database-target pair. Each dataset is indicated below the graph. Note

that all the Utah subjects in the original sample were male; we therefore did not replot the original data shown in Figure 1A here in panel(A).

Supplemental Figure 3. Self-correlation versus days between scans and age at scan 1 while separating subjects according to gender. In (A), the x-axis is days between scans; in (B), the x-axis is age at scan time 1. The y-axis is self-correlation (correlation of a subject from time 1 to time 2). Results of linear regression analyses are indicated in the appropriate graph.

Supplemental Figure 4. Self-correlation versus days between scans and age at scan 1 while separating subjects according to a 0.1 mm mean frame-frame displacement threshold. In (A), the x-axis is days between scans; in (B), the x-axis is age at scan time 1. The y-axis is self-correlation (correlation of a subject from time 1 to time 2). Results of linear regression analyses are indicated in the appropriate graph.

Supplemental Table 1. Results of partial correlation analyses. Dataset and scan pair are indicated in the leftmost column. The columns with headings X and Y indicate the variables included in the calculation of the sample linear partial correlation coefficient; Z indicates the variable being controlled for. Columns titled rho and p-val indicate the correlation coefficient and *p*-value, respectively.

Supplemental Table 2. Combined network 1 and 2 ID rates. Dataset is indicated in the leftmost column; note that session 1-session 2 data was used in this analyses. ID rate obtained, lower, and upper bounds of 95% confidence intervals are shown in the middle columns. Non-significant network pairs ($P > 0.05$) are indicated in the rightmost column.

	SLIM	Pitt	Utah
Subjects in session 1 and 2 (females)	105 (49)	93 (45)	26[a] (0)
Subjects in session 3 (females)	105 (49)	30 (16)[b]	-
Age at scan 1 (mean± SD)[c]	19.67 ± 0.96 years	15.23 ± 2.83 years	20.23 ± 8.28 years
Years between scan 1 and 2 (mean± SD)	0.84 ± 0.29 years	1.76 ± 0.41 years	2.54 ± 0.29 years
Years between scan 2 and 3 (mean± SD)	1.532± 0.18 years	1.53 ± 0.30 years	-
Years between scan 1 and 3 (mean± SD)	2.37 ± 0.28 years	3.16 ± 0.26 years	-
Scan duration in minutes (volumes)	8 (242)	5 (200)	8 (240)
TR in seconds	2	1.5	2

Table 1. Demographic and imaging characteristics of datasets used in this study.

a. The subjects in Utah session 2 contain two runs, hereafter referred to as 2A and 2B.
b. Scan session 2 and 3 occurred on the same day in one female subject in this session; we removed it when conducting analyses that required us to incorporate the number of days between scans 2 and 3.
c. All datasets provided age in years at scan session 1. For SLIM and Utah, the ages were reported as integers in years only, while the time between scan sessions was reported in days. To standardize the reporting of age among all three datasets, we only report age at session 1 here.

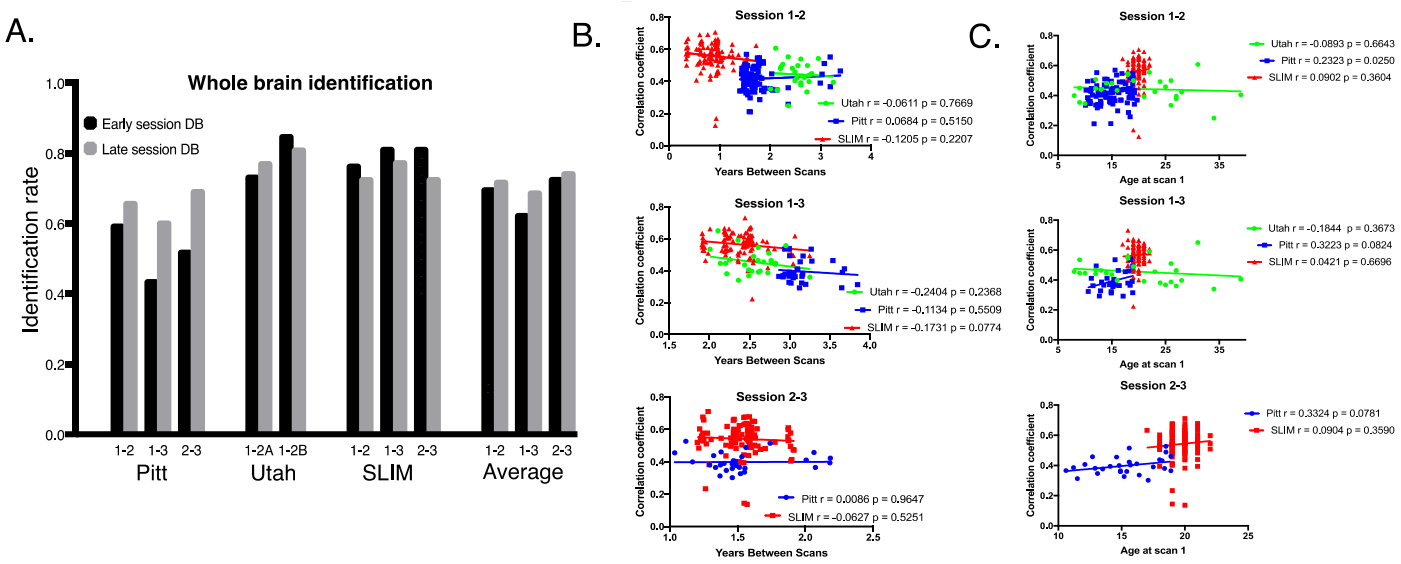

Figure 1. Connectome-based identification. Panel A: Results using whole brain data. Each dataset is indicated below the graph, along with the sessions that were involved in identification. Black shading indicates the early session served as the database session while the later session served as the target; gray shading indicates the later session served as the database with the early session serving as the target. "Average" refers to the average of all three datasets for each respective session identification pair. Panels B and C: Plotting self-correlation against years in between scans and age at scan time 1. Each dataset is indicated by the appropriate color and symbol. Results of linear regression analyses are shown on the appropriate graph.

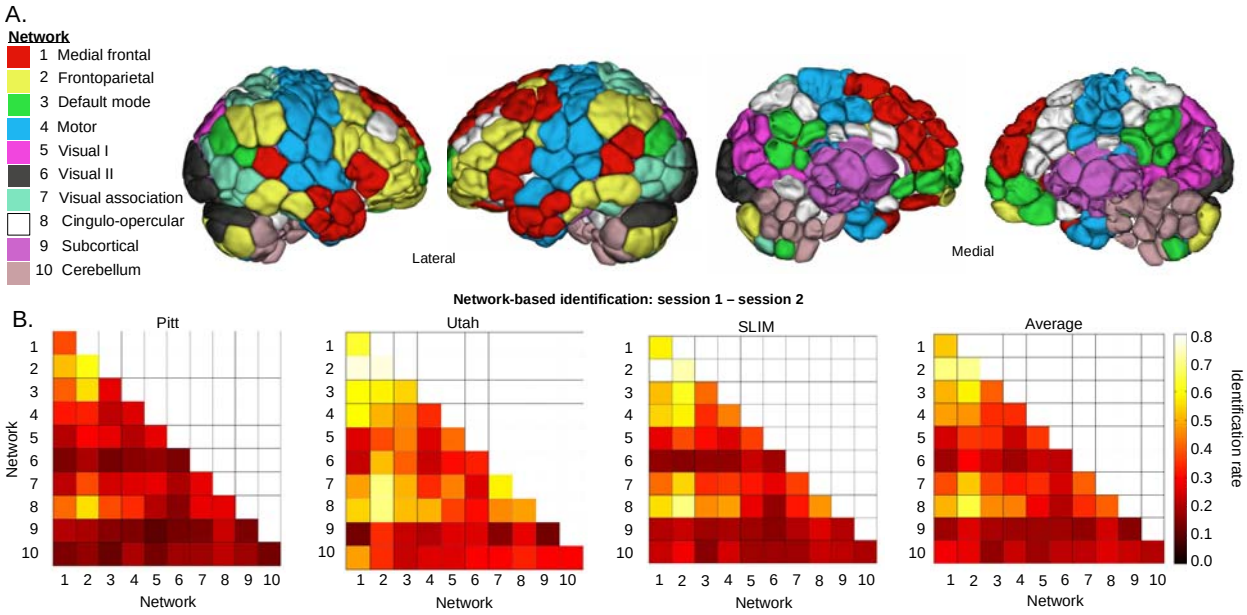

Figure 2. Network-based identification. Panel A: Node and network labels. We utilized a 268-node functional atlas. Nodes were further grouped into the 10 functional networks indicated here. Network names are to the left; anatomic locations are shown on the brains to the right. Panel B: We performed identification using only within- or between-network edges for session 1 and session 2 for all three datasets; shown are the average results for each database and target pair (i.e. a single element in the matrix represents the average identification rate of using session 1 as a database and session 2 as a target and vice-versa). “Average” above the right-most matrix refers to the average identification rate of all three datasets for session 1 and session 2 shown here. Note that because there were two scans in Utah session 2, we used session 2A in this analysis.

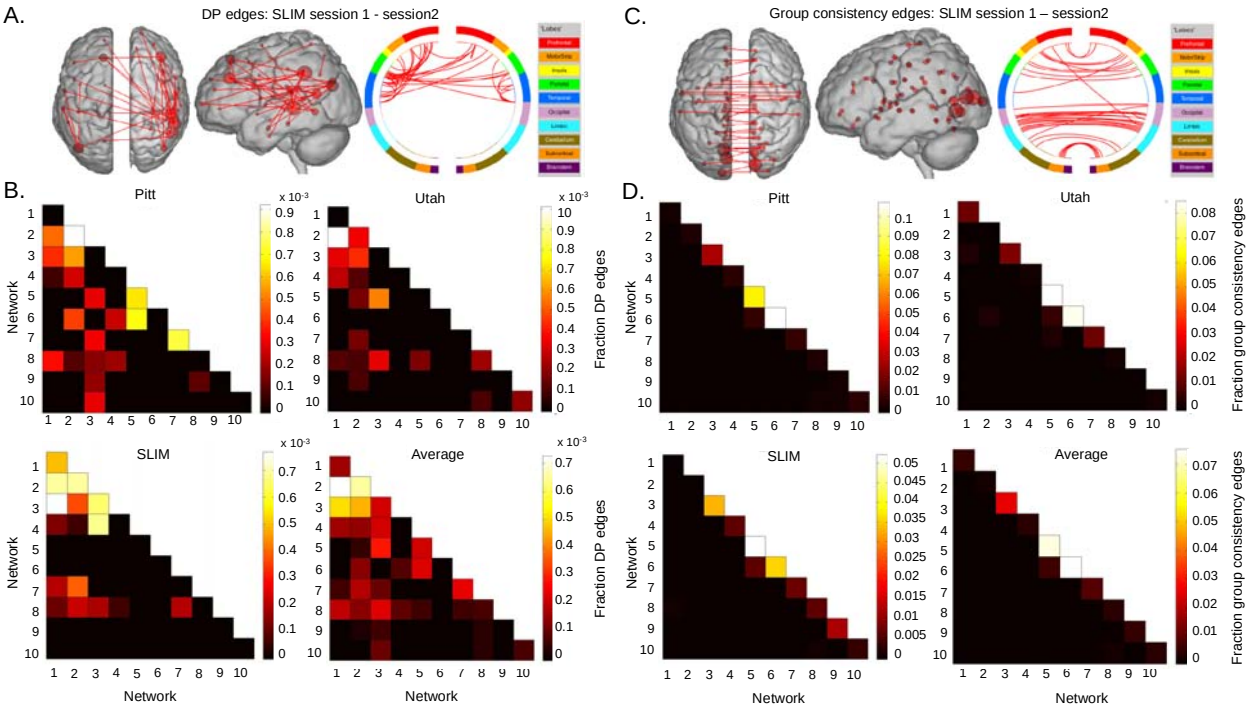

Figure 3. Results of edge-based analyses. Panel A: Anatomic location of highly unique (DP) edges from SLIM session 1-session 2. The edges shown here were in the top 99.9 percentile of highly unique edges. In the left two images of the brain, the red lines indicate edges connecting the red spheres, representing nodes. Nodes are sized according to degree, the number of edges connected to that node. On the right, the same nodes and edges are visualized on a circle plot, in which nodes are grouped according to anatomic location. The top of the circle represents anterior; the bottom, posterior. The left half of the circle plot corresponds to the left hemisphere of the brain. Panel B: Network representation of highly unique edges. Shown here are the data from the top 99.9 percentile of unique edges from session 1-session 2, as well as the average of all three datasets for session 1-session 2 shown here. Hotter colors indicate more edges are in the network pair. Note for both (B) and (D), the Utah session 2A scan was used. Panel C: Anatomic location of highly consistent (group consistency) edges from SLIM session 1-session 2. The edges shown here were in the top 99.9 percentile of highly consistent edges. Edges and nodes are represented as in (A). Panel D: Network representation of highly consistent edges. Shown here are the data from the top 99.9 percentile of highly consistent edges from session 1-session 2, as well as the average of all three datasets for session 1-session 2 shown here. The color scheme is as in (B). Note in (B) and (D) the scales of the color bars are not necessarily the same.